RSC Advances

Formation of PbO Hexagonal Nanosheets and Their Conversion into Luminescent Inorganic-Organic Perovskite Nanosheets: Growth and Mechanism

Journal:	*RSC Advances*
Manuscript ID:	RA-ART-01-2015-000809.R2
Article Type:	Paper
Date Submitted by the Author:	12-Mar-2015
Complete List of Authors:	Shakya, Suman; Indian Institute of Technology Delhi, Department of Physics G, Vijaya Prakash; IIT Delhi,

Formation of PbO Hexagonal Nanosheets and Their Conversion into Luminescent Inorganic-Organic Perovskite Nanosheets: Growth and Mechanism

Suman Shakya and G. Vijaya Prakash*

Nanophotonics Lab, Dept of Physics, Indian Institute of Technology Delhi, New Delhi 110016, India

Tel.: +91 11 26591326, email: prakash@physics.iitd.ac.in

Abstract:

We report the formation of inorganic-organic (IO) hybrid perovskite $(C_6H_9C_2H_4NH_3)_2$ PbI_4 hexagonal nanosheets, using anisotropically grown PbO hexagonal nanosheets as parent material. In place of conventional chemical synthesis route, the PbO hexagonal nanosheets have been synthesized by the bottom-up electrochemical deposition technique. Conversion of PbO into desired hybrid material has been achieved by the intercalation of organic moiety into the alternate layers of inorganic networks. These hybrid structures have shown the strong room-temperature excitonic emission at 518 nm. Extensive study has been performed to observe the deposition parameters responsible for the growth of a well-defined hexagonal nanosheet. High-resolution transmission electron microscope results confirmed the growth of single crystalline hexagonal nanosheets in (110) plane orientation. Investigation of surface morphology, further verified the formation of nanosheets with a smooth surface having an average roughness of 2 nm. The study revealed that the anisotropic growth of nanosheets is a result of different growth rate of crystal faces associated with crystal lattice.

Keywords: Perovskite materials, nanosheets, electrochemical deposition, inorganic-organic hybrid materials, self-assembly.

Introduction:

In this era of novel technological materials, inorganic-organic (IO) hybrid semiconductors play key role for their applications in photonic materials, miniaturized sensors, non-linear optical elements, optoelectronics devices by utilizing the properties of both the mediums in a single entity[1-5]. Similarly, ordered structures of nanomaterials have drawn significant research interest, since such materials give rise to many unique and enhanced properties in comparison to their bulk counterparts[6]. In the special class of novel nanomaterials, inorganic-organic hybrid materials are of unique structures, considered to be a molecular or nanocomposites where the dimension of at least one its constituent should be in a range from few angstroms to several nanometers. The combined properties of inorganic (such as high carrier mobility, low resistivity) and organic (such as accessibility to tunable properties and easy of fabrication) moieties make them promising candidate for many optoelectronics applications[4,7-10]. One of the popular class of IO nano-hybrid materials are represented with the general formula AMX_3, where A= organic moiety, M = metals (Pb^{2+}, Sn^{2+}, etc) and X = halides (I^-, Br^- or Cl^-)[4,11]. Changing the size, functionality and shape of intercalated organic moiety, these materials can possess 1D, 2D and 3D extended crystal network[12]. Due to the low dimensionality and band gap contrast between inorganic and organic material, IO hybrids give rise to the large dielectric mismatch. Based on the dimensionality of these materials, among them 2D IO hybrid materials ($(R\text{-}NH_3)_2\ MX_4$ (where R is organic moiety) exhibit strong excitonic photoluminescence with narrow band width[13,14]. One the other hand, Lead oxide (PbO) is a good candidate for many applications ranging from batteries, rubber industry to photovoltaics[15-17]. Depending upon the oxidation states

lead oxide adopts four forms (PbO, PbO_2, Pb_2O_3 and Pb_3O_4). Among all, lead oxide PbO is notably important because of its optoelectronic properties[18,19], exists in two crystal structure[15]. For the fabrication of PbO several fabrication techniques have been used, namely, thermal deposition[15], laser-assisted deposition[20], solvothermal route[21], sonochemical[22] and hydrothermal methods[23]. Among other fabrication techniques electrochemical deposition is a versatile, cost-effective technique which allows changing the properties by slight variation of the deposition parameters without any requirement of further processing or sophisticated environment[24]. Recently, our group has reported straight forward methodology to deposit $((R\text{-}NH_3)_2\ MX_4$ type hybrid thin film from simple three step method[1,25-27]. Though PbO thin film fabrication is widely known, to the best of our knowledge, no literature has been reported the fabrication of PbO hexagonal nanosheets by electrochemical deposition technique.

In this report, we have demonstrated the formation of hexagonal PbO nanosheets and explained the possible mechanism behind its growth. Optimization of growth parameters have been studied with the variation of responsible deposition conditions. Using scanning electron microscope (SEM) and high-resolution transmission electron microscope (HRTEM) techniques, nucleation and growth process have been analyzed. Optimized growth parameters have been implemented to fabricate PbO hexagonal nanosheets, finally the desired IO hybrid material is obtained by conversion of PbO into PbI_2 and then intercalation of organic moiety[25-27].

Experimental Details:

PbO hexagonal nanosheets were grown using aqueous solution of 2 mM lead acetate ($Pb(CH_3COO)_2$) and 0.1 M sodium acetate (CH_3COONa) as precursors, at the pH value of 6.6. Three electrodes setup was used for the deposition, wherein saturated calomel electrode and

platinum mesh were used as reference and counter electrode respectively. ITO coated glass acted as working electrode. Cyclic voltammetry (CV) was performed to get a range for deposition potential of PbO. To understand the growth of well-defined hexagonal nanosheets, various parameters were optimized. To observe the effect of pH, 5% HNO_3 solution was used to vary the pH value (from 4 to 6) of the electrolytic bath. X-ray diffraction (XRD) of the material was performed (Philips Panalytical X'Pert Pro) using Cu-Kα source. The shape and size of the hexagonal nanosheets at various parameters were studied by Scanning Electron Microscope (SEM) (Evo50 XVP Carl Zeiss). To confirm the elemental composition of the nanosheets over an area, elemental mapping and spectra were recorded using Energy-dispersive X-Ray Spectroscopy (EDX) equipped with SEM. High Resolution Transmission Electron Microscopy (HRTEM) (Tecnai G20-Stwin at 200KV) was used to confirm size as well as the single crystalline structure of individual hexagonal nanosheet. Surface roughness and height of a nanosheet has been studied by Atomic Force Microscopy (AFM) (Dimension Icon Model, Bruker).

To synthesize the desired inorganic-organic hybrid, further, the as-deposited PbO was thermally exposed to iodine vapors in a closed chamber for 3 minutes to convert it into PbI_2 and finally 2-(1-Cyclohexenyl) ethyl ammonium iodide, $C_6H_9C_2H_4NH_3I$ (CHI) organic moiety solution (40 mg in 5 ml toluene) was used to intercalate into PbI_2 to form the titled IO hybrid, i.e. 2-(1-Cyclohexenyl) ethyl ammonium lead iodide, (hereafter, CHPI).

Results and discussion:

The growth of PbO hexagonal nanosheets was optimized by modifying various parameters. Cyclic voltammetry was performed to optimize the deposition potential range. Fig.S1 shows (see

in supplementary information) the cyclic voltammogram (CV) for the redox cycle of PbO, point (a) on the graph, is the potential from where reduction of lead ions (Pb) started. From the CV, the deposition potential range for PbO is found out to be 1.3 V to 0.8 V. Based on this observation, deposition potential has been systematically varied over the given range during the deposition of PbO on ITO coated glass substrate to observe the effect of deposition potential on the growth of hexagonal nanosheets. The XRD pattern (Fig S1 (b)) (see in supplementary information) recorded for the deposited PbO confirmed the orthorhombic phase of β-PbO (JCPDS No.76-1796). The strong reflections of 2θ values at 24.755°, 29.175°, 30.375° corresponds to (110), (111) and (002) planes respectively. Due to the exposure of sample into the air, the conversion of PbO into Pb_3O_4 is indicated by a small peak at 26.378° along with ITO substrate peak at 35.33°.

The SEM images of PbO nanosheets (Fig. 1), shows the nucleation and growth rate at different deposition potentials for the deposition time of 15 minutes. SEM images reveal that, at 0.9 V agglomerated clusters of small PbO particles were observed. With the increase in potential, clusters started to grow into the desired hexagonal nanosheets (shown in Fig. 1(b)).

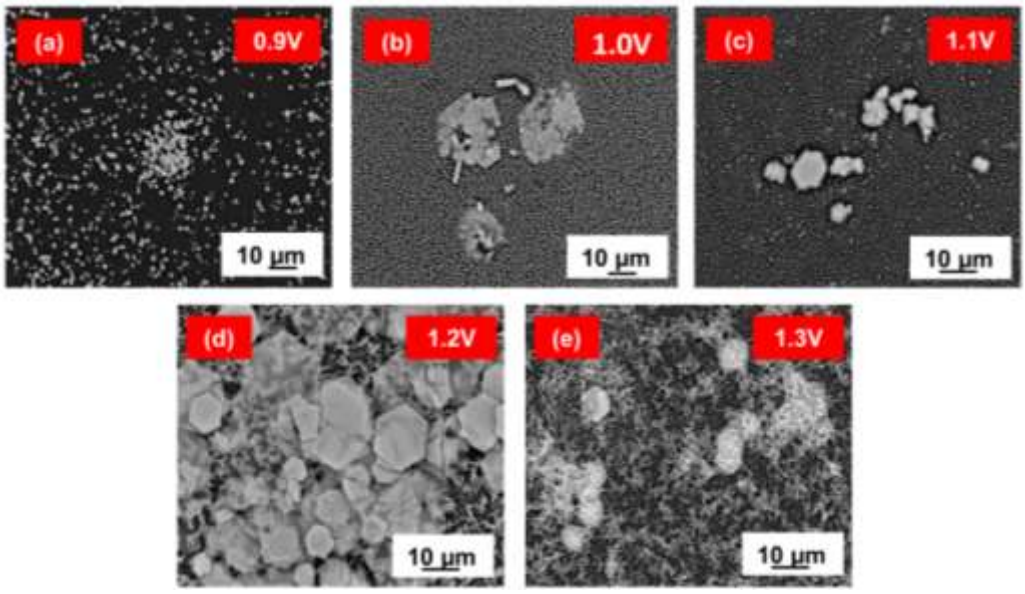

Fig.1 (a-e) SEM images of PbO nanosheets for the deposition time of 15 minutes, showing the effect of deposition potential on the growth nanosheets at 0.9V, 1.0 V, 1.1 V, 1.2 V and, at 1.3 V potentials respectively at constant pH= 6.6 .

From the deposition potential 1.0 V, formation of deformed PbO hexagonal nanosheets can be observed. At the deposition potential 1.2 V, well-defined hexagonal structured nanosheets formed over the larger areas, up to 100 μm^2. By applying more potential i.e. at 1.3 V, fern-like hexagonal structures are observed, which signs towards the over-growth due to the large charge drawn during deposition. By optimizing the deposition potentials, it can be concluded that well-shaped hexagonal nanosheets can be obtained at 1.2 V over a reasonably larger area. Further, to study the time evolution of PbO hexagonal nanosheet growth, deposition was carried out at different time durations, starting from 5 min to 40 min (at 1.2 V). After the deposition for 5 minutes, SEM images in Fig.2(a) shows that the nucleation process started which led to the self-assembly of nanoparticles at the expense of smaller clusters of PbO particles.

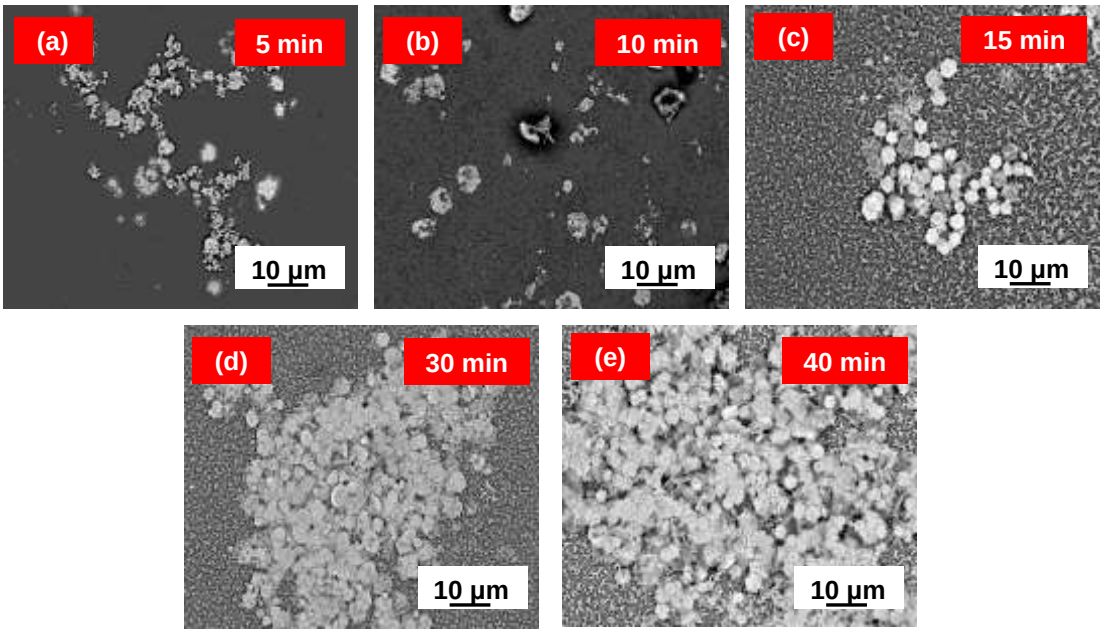

Fig.2 SEM images of nanosheets showing the nucleation and growth process during various deposition times, (a)5 min, (b)10 min, (c)15 min, (d) 30 min and (e) 40 min respectively. The deposition potential is fixed at 1.2 V at constant pH= 6.6 .

From Fig.2, it is convenient to conclude that well shaped hexagonal nanosheets started to grow from the deposition duration of 10 minutes. With the increase in deposition time, growth of nanosheets increased up to certain size, the average dimension of nanosheets were found in the range of 4-5 micron (shown in Fig.2(d)). Further increment in deposition time, more than 30 min, c-axis growth of nanosheets had been saturated and only the lateral dimensions of nanosheets increased. Besides the deposition potential and time, there are some other factors which play significant role in the deposition by electrodeposition method. To elaborate the growth study, pH and concentration of the electrolytic solution were also changed to anticipate their roles. From the SEM images of Fig.S2 (a-c) (see in supplementary information) , it can be interpreted that that lowering the pH value of the electrolytic bath inhibits the growth of hexagonal nanosheets and leads to the growth of irregular fern-like structures. Further, to

investigate the effect of the concentration of lead acetate in the electrolytic bath deposition was performed for high concentration(0.5 M) of lead acetate. From the SEM images, Fig.S2 (d) (see in supplementary information), it can be predicted that, as lead acetate is expected as electrochemically inert, excess concentration of the same slow down the process of nucleation and inhibits further growth.

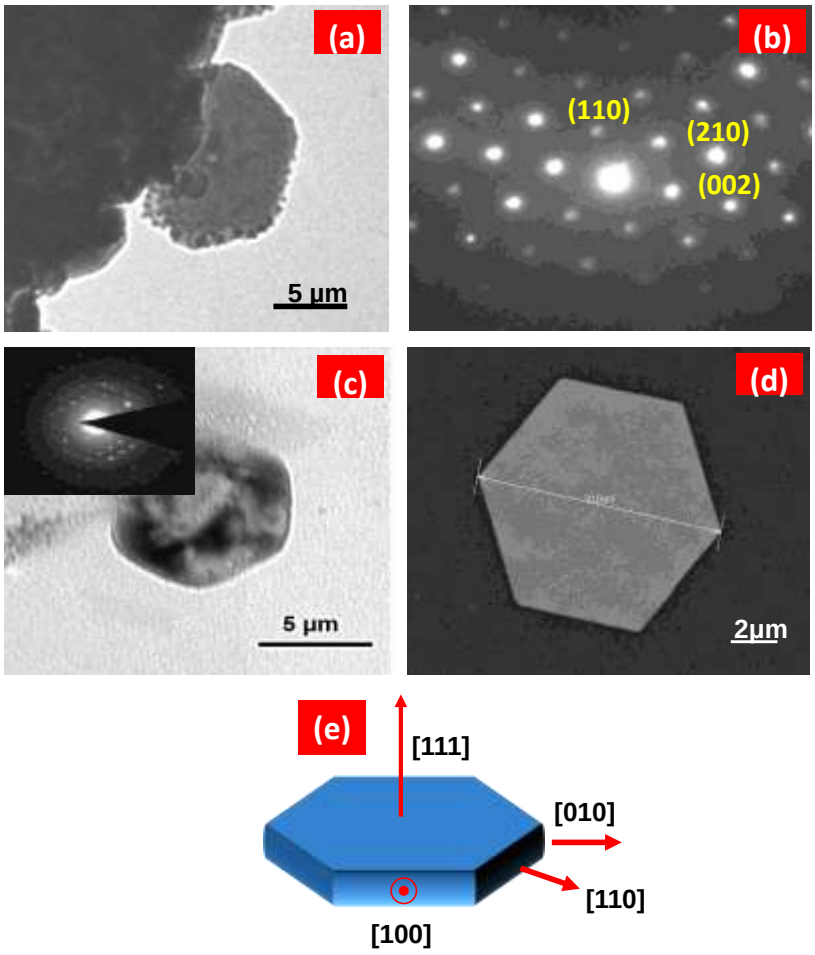

Fig.3 (a) and (c) shows the HRTEM images of a hexagonal nanosheet for the deposition time of 5 and 10 minutes respectively. (b) and inset of (c) shows the respective selected area electron diffraction (SAED) patterns along [111] zone axis. (d) shows the SEM image of a single

hexagonal nanosheet (of size ~ 10μm) and (e) shows schematic representation of PbO crystal directions [111], [110], [010] and [100].

To get the insight of morphology and the crystal structure of the nanosheets, HRTEM was utilized for the study. Fig.3 (a) & (c) shows the HRTEM images of a single nanosheet obtained after the deposition time of 5 minutes and 10 minutes respectively. On close inspection of the micrograph (Fig.3 (a)), at the edges of the nanosheet agglomerated small nanoparticles can be observed, suggesting the initiation of nucleation, which is also may be due to the oxidization of nanosheet from PbO to Pb_3O_4. Whereas after 10 minutes full-grown hexagonal nanosheet was formed (Fig. 3(c)). Fig.3 (b) and inset of Fig.3 (c) show the SAED pattern corresponding along the [111] zone axis of the nanosheet, indicating that the upper surface of the hexagonal nanosheet is (111) crystal plane. The dotted SAED pattern is the evidence of the single crystalline structure of the nanosheets, on which (110), (210) and (002) planes have been indexed (Fig. 3(b)). The calculated d-spacing for (110), (210) and (002) planes are 0.35 nm, 0.29 and 0.24 nm respectively, which are in a very good agreement with the XRD result (Fig. S1).

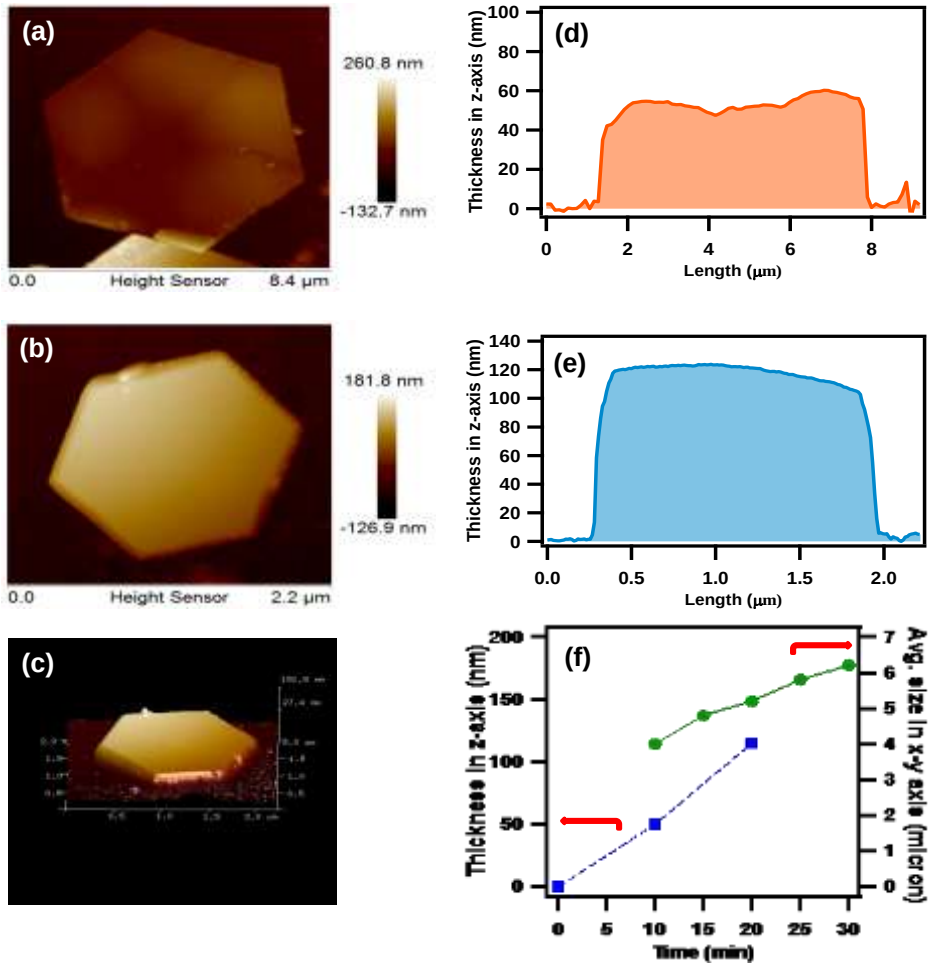

158

159 *Fig.4 (a) & (b) Atomic Force Microscopic images of hexagonal structured PbO nanosheet for*
160 *the deposition time of 10 minutes and 20 minutes respectively, (d) & (e) shows the corresponding*
161 *height profile of the same respectively, (c) shows the 3-dimensional AFM image of nanosheet*
162 *and (f) is the plot showing thickness and average lateral size of hexagonal PbO nanosheets for*
163 *various deposition time.*

164 To examine the surface morphology of the nanosheet with the duration of time, AFM
165 characterization was employed. From the Fig.4 (d) & (e), the thickness of nanosheet after the
166 deposition time for 10 and 20 minutes was found to be ~ 60 and 120 nm respectively. Average
167 surface roughness of the nanosheet was found to be 2 nm over a large area of 1μm^2, which

signifies the high quality of nanosheet formation with less surface flaws. Fig. 4 (f) is giving the quantitative parameters for the growth of nanosheets, shows that initially nanoparticles self-assembled to grow in lateral dimension (along [110] direction) and after 5 minutes nanosheet started to grow faster along [110] direction as well as slower growth was also followed along c-axis, i.e. [111] direction. The thickness of nanosheets along c-axis were observed ~ 60 nm and up to a thickness of ~ 120 nm for the deposition time of 10 minutes and 20 minutes respectively (Fig.4 (f)), further growth of nanosheet saturated along z-axis (i.e., thickness) after 20 minutes of deposition. The average size of nanosheets in the lateral dimension was found to be 5 μm for optimum deposition conditions.

Further, to investigate the elemental quantification of nanosheets, EDX was also performed. EDX equipped with a SEM was used to record the spectrum on a selected area covered by nanosheets only, for precise analysis of weight percentage of the nanosheets. Energy-dispersive X-ray spectrum of the nanosheets in Fig.5 (a) shows the characteristic peaks of Lead (Pb) and Oxygen (O). The elemental weight percentage of nanosheets is given in Table S1, according to the weight percentage of Pb and O found in the nanosheets, the formation of PbO compound can be substantiated. As nanosheets were dispersed over the ITO substrate, EDX mapping was performed over the deposited area to quantify the elemental contrast over the whole region. Fig.5 (c) & (d) shows the EDX mapping corresponds to lead and oxygen respectively, from the mapping it is evident that the color contrast between lead and oxygen is in agreement with the weight percentage given in Table S1 (see in supplementary information).

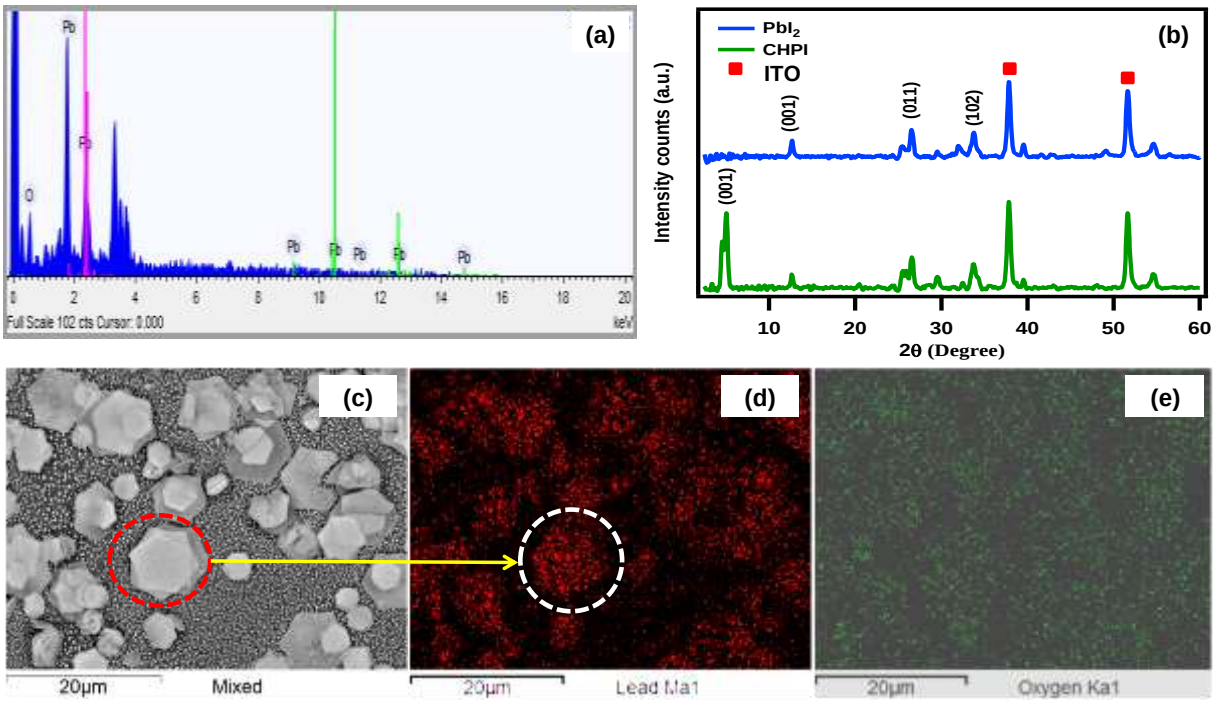

Fig.5 (a) EDX spectra of PbO hexagonal nanosheets, (b) shows the XRD pattern for converted PbI_2 and CHPI. (c) is SEM image of PbO hexagonal nanosheets and (d) & (e) are corresponding EDX elemental area mappings for lead and oxygen respectively.

The aforementioned studies reveal that the formation of desired hexagonal nanosheets requires precise optimization of deposition parameters and critical understanding of growth process. The nanosheets growth has been first initiated along the lateral directions corresponds to (110) plane and after 10 minutes, nanosheets started growing in c-axis also (as shown in Fig.2). As seen from figure 3a, initially for the deposition time of 5 minutes, agglomerated clusters of PbO nanoparticles observed to form a premature stage of hexagonal shaped nanosheets. As the time increases, the edges of the premature PbO nanosheets tend to develop and after 15 min of deposition time, the PbO grew over larger area into well-defined hexagonal nanosheets. Further increasing the deposition time (above 20 minutes) there is minimum change in the c-axis growth

of PbO nanosheets along with the growth of fern-like structures in the background. However, from the SEM images (Fig. 1 & 2) it is also evident that the growth is not continuous. The reason for non-uniform surface coverage of hexagonal nanosheets over large area can be understand with the fact that ITO substrate may not have homogeneous conduction across the surface due inhomogeneous sheet resistance. Further, the nanosheets have been found to be deposited over the small nanoparticles, which indicate that the growth of hexagonal nanosheets is a result of secondary nucleation on the substrate (see Fig.S3 in supplementary results). The formation of hexagonal nanosheets is related to the difference in growth rate of various crystal faces bound to the crystal lattice, as discussed by Laudise et al[28]. The growth mechanism of oxide crystals depends upon the orientation of different coordination polyhedron at different crystal interfaces of neighboring atoms. Therefore, the growth rate of crystal faces will be different at different interfaces[29]. Here, the growth of nanosheets is predicted as a result of different growth rates at different crystal interfaces. Apart from coordination polyhedron, the local environment of the solution at substrate also play crucial role in electrochemical deposition. Applied potential dissociate ions from the solution and draws reduced Pb^{2+} anions and O^{4-} cations towards substrate due to coulombic attraction. In electrochemistry, for the proper deposition of binary or ternary semiconductors, deposition parameters should be optimized individually, therefore the role of concentration of reactants or additives is predominant[30]. In a similar growth study reported by Schliehe et al[31], the growth of PbS nanosheets is perpendicular to [111] facet. On the basis of this study, we believe that during the formation of sheet-like structure, the growth happens faster perpendicular to the most energetic unfavorable facet, which is consumed to lower the surface energy of clusters. Here, the growth of nanosheet progressed in the perpendicular direction to the high surface energy facet, i.e. [111] direction as shown in Fig. 3(e).

Finally, the luminescent inorganic-organic (IO) hybrid CHPI nanosheets are fabricated from a three step process[10,25], which involves (a) formation of PbO nanosheets using above listed optimized parameters, (b) iodinization of PbO nanosheets to convert them into PbI_2 and (c) the conversion of PbI_2 into IO hybrid CHPI nanosheets by the intercalation of organic moiety (CHI). The resultant PbI_2 and CHPI materials XRD patterns are shown in Fig.5 (b), evidenced the conversion of PbO into hexagonal crystal structured PbI_2. It is known that PbI_2 is a 2D layered structure oriented along c-axis[7], which is confirmed by strong diffraction from (001) plane. As, PbI_2 is a layered structure, intercalation of organic moiety (CHI) into PbI_2 leads to alternate stacking of organic moiety with inorganic semiconductor layers, which resulted in a inorganic-organic hybrid structure[1]. In the XRD pattern (Fig.5(b)) of CHPI, diffraction peak from (001) plane assured the intercalation of CHI into PbI_2 layers, some peaks of PbI_2 have been observed, which can be attributed to the fact that the intercalation process was not fully completed..

Intercalation time should be optimized[32] to sustain the original shape of structure, Fig. 6(a) shows the SEM images of intact PbI_2 and CHPI hexagonal nanosheet for the intercalation time of 5s, which sustain the original structure after all the chemical processes. As the result of intercalation, nanosheets swelled minutely. Due to the low dimensionality[8], these IO hybrid structures show strong and narrow room temperature excitonic photoluminescence (PL) at 518 nm when excited with 410 nm wavelength (Fig 6(e)). Fig.6(b), (c) & (d) shows confocal microscopic images of well-shaped CHPI nanosheets in white light, bright field image in white light along with 410 nm excitation wavelength and photoluminescence image emitting green color respectively. As the nanosheets were scattered over the substrate, to get a larger view, microscopic images were taken at lower magnification of objective eyepiece (at 20X). Fig.S4 (a-d) (see in supplementary information) shows the confocal microscopic white light image of PbO

hexagonal nanosheets, white light image of CHPI IO hybrid nanosheets, white light image along the excitation with 410 nm wavelength and photoluminescence image of the same.

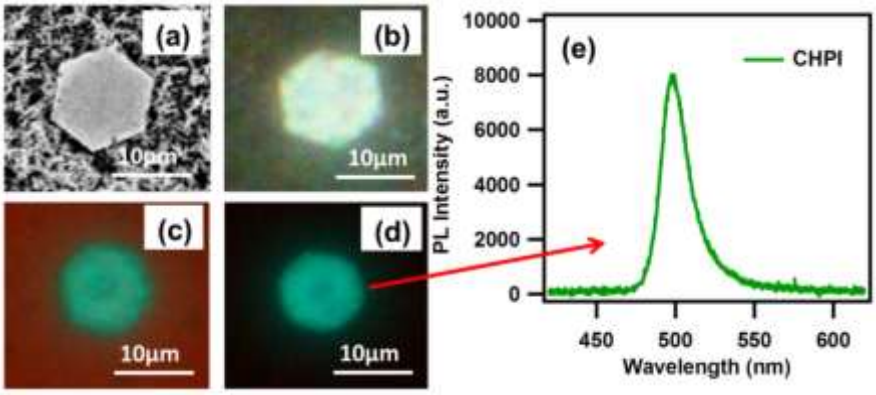

Fig.6 (a) SEM image, (b) confocal microscopic white light and (c) combined white light + PL image and (d) PL image of a single CHPI nanosheet. Figure (g) is PL spectra of individual CHPI nanosheet. The excitation wavelength for PL is 410 nm and the PL images are obtained using a 420 nm long pass filter.

Conclusion:

We have reported the formation of well-defined hexagonal nanosheets using electrodeposition technique, and their conversion into luminescent CHPI IO hybrid material by the intercalation of organic moiety into the layered structure of inorganic nanosheets. To completely understand the factors leading to the growth of hexagonal PbO nanosheet structure, deposition parameters have been explicitly studied. HRTEM results and SAED pattern indexing confirmed the growth of single crystalline PbO nanosheets occurred in the direction parallel to (111) plane, which resulted in a sheet-like structure. Further, to examine the surface quality of nanosheets, AFM has been employed to provide the average surface roughness over a larger area (1 μm^2), which was found

265 to be ~2 nm. Finally, these electrodeposited hexagonal PbO nanosheets has been converted into
266 luminescent CHPI by simple three step process.

267 **ASSOCIATED CONTENT**

268 **Supplementary Information**

269 Figure S1: Cyclic voltammogram of electrolyte solution used for deposition and X-ray
270 diffraction pattern of as-deposited PbO film. Table S1 shows the percentage of elemental
271 composition of PbO nanosheets given by EDX result. Figure S2 shows the effect of pH and
272 concentration of precursors in the deposition bath. Figure S3 shows the growth of hexagonal
273 nanosheets as a result of secondary nucleation on the substrate. Figure S4 shows the white light
274 confocal microscopic images of PbO hexagonal nanosheets and photoluminescence images of
275 converted inorganic-organic perovskite nanosheets.

276 **ACKNOWLEDGE**

277 This work is supported by High-Impact Research scheme of IIT Delhi, Nano Research Facility
278 (MCIT, Govt. Of India), Department of Science and Technology (DST) project and UK-India
279 Education and Research Initiative (UKIERI) programme,.

280

281

282

283

284

References:

(1) S. Ahmad, P. K. Kanaujia, W. Niu, J.J. Baumberg, G. Vijaya Prakash, *ACS Appl. Mater. Interfaces* 2014, **6(13)**, 10238-10247.

(2) S. Ahmad, C. Hanmandlu, P. K. Kanaujia, G. Vijaya Prakash, *Opt. Mater. Express* 2014**, 4(7)**, 1313-23.

(3) M. Era, S. Morimoto, T. Tsutsui, and S. Saito, *Appl. Phys. Lett.*, 1994, **65 (6)**, 676-678.

(4) H. Snaith, *J. Phys. Chem. Lett.*, 2013, **4**, 3623–3630.

(5) P.P. Boix, K. Nonomura, N. Mathews, and S.G. Mhaisalkar, *Mater. Today*, 2014, **17(1)**, 16-23.

(6) Q. Wang, X. Sun, S. Luo, L. Sun, X. Wu, M. Cao, C. Hu, *Cryst. Growth Des.* 2007, **7**, 2665-2669.

(7) K. Pradeesh, J.J. Baumberg, and G. Vijaya Prakash, *Appl. Phys. Lett.*, 2009, **95**, 033309-1-3.

(8) T. Ishihara, J. Takahashi, and T. Goto, *Phys. Rev. B*, 1990, **42(17)**, 11099-11107.

(9) C. C. Stoumpos, C. D. Malliakas, and M. G. Kanatzidis, *Inorg Chem*, 2013, **52**, 9019–9038.

(10) V.K. Dwivedi and G. Vijaya Prakash, *Solid State Sci.*, 2014, **27**, 60-64.

(11) D. Mitzi, *J. Chem. Soc., Dalton Trans.*, 2000, **1**, 1-12.

(12) D.G. Billing and A. Lemmerer, *New J. Chem.*, 2008, **32**, 1736-1746.

(13) K. Pradeesh, J.J. Baumberg, and G. Vijaya Prakash, *J. Appl. Phys.*, 2012, **111**, 013511-1-6.

(14) T.L. Blair, J. *Power Sources* 1998, **73(1)**, 47-55.

(15) L.M. Droessler, H.E. Assender, A.A.R. Watt, *Mater. Lett.* 2012, **71**, 51-53.

(16) L. Zhang, F. Guo, X. Liu, J. Cui, and Y. Qian, *J. Cryst. Growth*, 2005, **280**, 575-580.

(17) J. C. Schottmiller, *J. of Appl. Phys.*, 1966, **37**, 3505–3510.

(18) J. Berashevich, O. Semeniuk, O. Rubel, J.A. Rowlands, and A. Reznik, *J. Phys.: Condens. Matter*, 2013, **25**, 075803-1-7.

(19) H.J. Terpstra, R.A. de Groot, C. Hass, *Phy. Rev. B* 1995, **52(16)**, 11690-11697.

(20) M. Baleva, V. Tuncheva, *J. Mater. Sci. Lett.* 1994, **13**, 3-5.

(21) P. Gao, Y. Liu, X. Bu, M. Hu, Y. Dai, X. Gao, and L. Lei, *J. Power Sources*, 2013, **242**, 299-304.

(22) H. Haddadian, A. Aslani, A. Morsali, *Inorg. Chim. Acta* 2009, **362**, 1805-1809.

(23) Y. Wang, X. Lin, H. Zhang, T. Wen, F. Huang, G. Li, Y. Wang, F. Liao, J. Lin, *CrystEngComm* 2013, **15(18)**, 3513-3516.

(24) S. Shakya, G. Vijaya Prakash, *Mater. Res. Express* 2014, **1**, 035037-1-11.

(25) V.K. Dwivedi, J. J. Baumberg, G. Vijaya Prakash, *Mater. Chem. Phys.* 2013, **137**, 941-946.

(26) W. Niu, A. Eiden, G. Vijaya Prakash, and J.J. Baumberg, *Appl. Phys. Lett.*, 2014, **104(17)**, 171111-1-4.

(27) J.H. Heo, S.H. Im, J.H. Noh, T.N. Mandal, C.S. Lim, J.A. Chang, Y.H. Lee, H. Kim, A. Sarkar, M.K. Nazeeruddin, M. Grätzel, and S. Seok, *Nature Photon.*, 2013, **7**, 486-491.

(28) R.A. Laudise and A.A. Ballman, *J. Phys. Chem.*, 1960, **65(5)**, 688-691.

(29) W.J. Li, E.W. Shi, W.Z. Zhong, and Z.W. Yin, *J. Cryst. Growth*, 1999, **203**, 186–196.

(30) E.M. Mkawi, K. Ibrahim, M.K.M. Ali, M.A. Farrukh, A.S. Mohamed, and N.K. Allam, *J. Electroanal. Chem.*, 2014, **735**, 129-135.

(31) C. Schliehe, B.H. Juarez, M. Pelletier, S. Jander, D. Greshnykh, M. Nagel, A. Meyer, S. Foerster, A. Kornowski, C. Klinke, H. Weller, *Science (New York, N.Y.)* 2010, **329**, 550–553.

(32) I. Saikumar, S. Ahmad, J. J. Baumberg, G. Vijaya Prakash, *Scripta Mater.* 2012, **67**, 834-837.